Electronic Supplementary Information

for

A stable and true-blue emissive hexacoordinate Si(IV) N-heterocyclic carbene complex and its use in organic light-emitting diodes

Thibault Thierry [†,a], Valerio Giuso [†,a], Federico Polo,[b,c] Pierluigi Mercandelli,[d] Yi-Ting Chen,[e]

Chih-Hao Chang,[e] Matteo Mauro*[a] and Stéphane Bellemin-Laponnaz*[a]

[a] Université de Strasbourg & CNRS, Institut de Physique et Chimie des Matériaux de Strasbourg (IPCMS UMR 7504) F-67034 Strasbourg, France

[b] Department of Molecular Sciences and Nanosystems, Ca' Foscari University of Venice, Via Torino 155, 30172 Venice, Italy.

[c] European Centre for Living Technology (ECLT), Ca' Foscari University of Venice, Ca' Bottacin, 30124, Venice, Italy.

[d] Università degli Studi di Milano, Dipartimento di Chimica, 20133 Milan, Italy

[e] Department of Electrical Engineering, Yuan Ze University, 32003 Taoyuan, Taiwan

* Corresponding authors

Email of corresponding authors:

Stéphane Bellemin-Laponnaz: bellemin@unistra.fr

Matteo Mauro: mauro@unistra.fr

† T.T. and V.G. have equally contributed to this work.

Contents

General experimental remarks

All reagents and solvents were purchased from commercial chemical suppliers (Acros, Alfa Aesar, Sigma-Aldrich and TCI Europe) and used without further purification, except for benzaldehyde which was distilled and stored under argon prior to use. Deuterated chloroform NMR solvent was stored over 4Å molecular sieves. NMR spectra were recorded with a 300 or 500 MHz apparatus in deuterated solvent at 25°C. All ^{13}C NMR spectra are decoupled ^{1}H ($^{13}C\{^{1}H\}$). The chemical shifts (δ) and coupling constants (*J*) are expressed in ppm and Hz respectively. The following abbreviations are used: s: singlet; d: doublet; t triplet; q: quadruplet; quint: quintuplet; sext: sextet; sept: septet; m: multiplet; br: broad signal.

Synthesis of **Si(OCO)$_2$** :

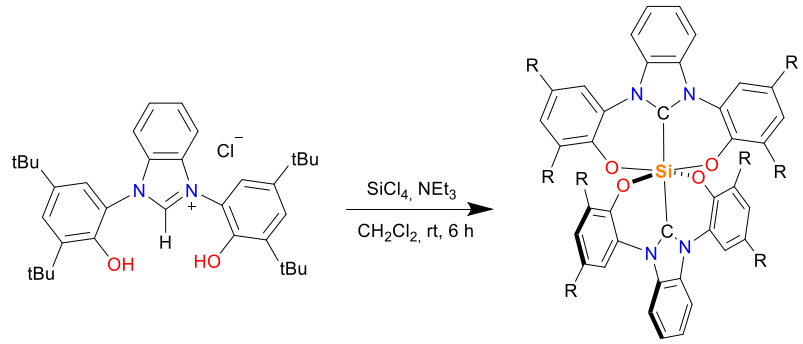

(OCO)H$_3$ **Si(OCO)$_2$**

Scheme S1. Synthetic procedure employed for the preparation of compound **Si(OCO)$_2$**

To a DCM (6 mL) solution of the **(OCO)H$_3$** ligand[1] (200 mg, 0.35 mmol, 2 eq.) in a schlenk tube was introduced a 1M DCM solution of $SiCl_4$ solution (175 μL, 0.175 mmol, 1 eq.), under argon at rt. After 15 min of stirring, NEt_3 (123 μL, 0.875 mmol, 5 eq.) was added dropwise, and the medium was stirred during 6 h. After evaporation of the DCM, toluene was added to the crude product and the mixture was filtered to eliminate NEt_3Cl. The filtered solution was concentrated under reduced pressure and the crude product was purified by column chromatography on silica gel using pentane/DCM (50/50 up to 0/100 gradient). The desired product was obtained in 78% yield (152 mg, 0.137 mmol)

^{1}H NMR (500 MHz, $CDCl_3$) δ 8.29 (dt, $^{3}J_{HH}$ = 6.7, $^{3}J_{HH}$ = 3.4 Hz, 4H), 7.83 (d, $^{3}J_{HH}$ = 2.3 Hz, 4H), 7.59 (dt, $^{3}J_{HH}$ = 6.7, $^{3}J_{HH}$ = 3.4 Hz, 4H), 7.10 (d, $^{3}J_{HH}$ = 2.3 Hz, 4H), 1.34 (s, 36H), 0.72 (s, 36H). **^{13}C NMR** (126 MHz, $CDCl_3$) δ 165.3(2C), 150.0 (4C), 141.0 (4C), 138.0 (4C), 130.9 (4C), 125.6 (4C), 124.9 (4C), 121.9 (4C), 115.0 (4C), 114.7 (4C), 34.8 (4C), 34.5 (4C), 31.8 (12C), 29.2 (12C). **^{29}Si NMR** (99 MHz, $CDCl_3$) δ -197.43. **HRMS** (ESI+, m/z) $[M+H]^+$ calculated for $C_{70}H_{89}N_4O_4{}^{28}Si$ 1077.66476 found 1077.6635. **TGA**: 5% weight loss at $T_{5\%}$ = 350°C

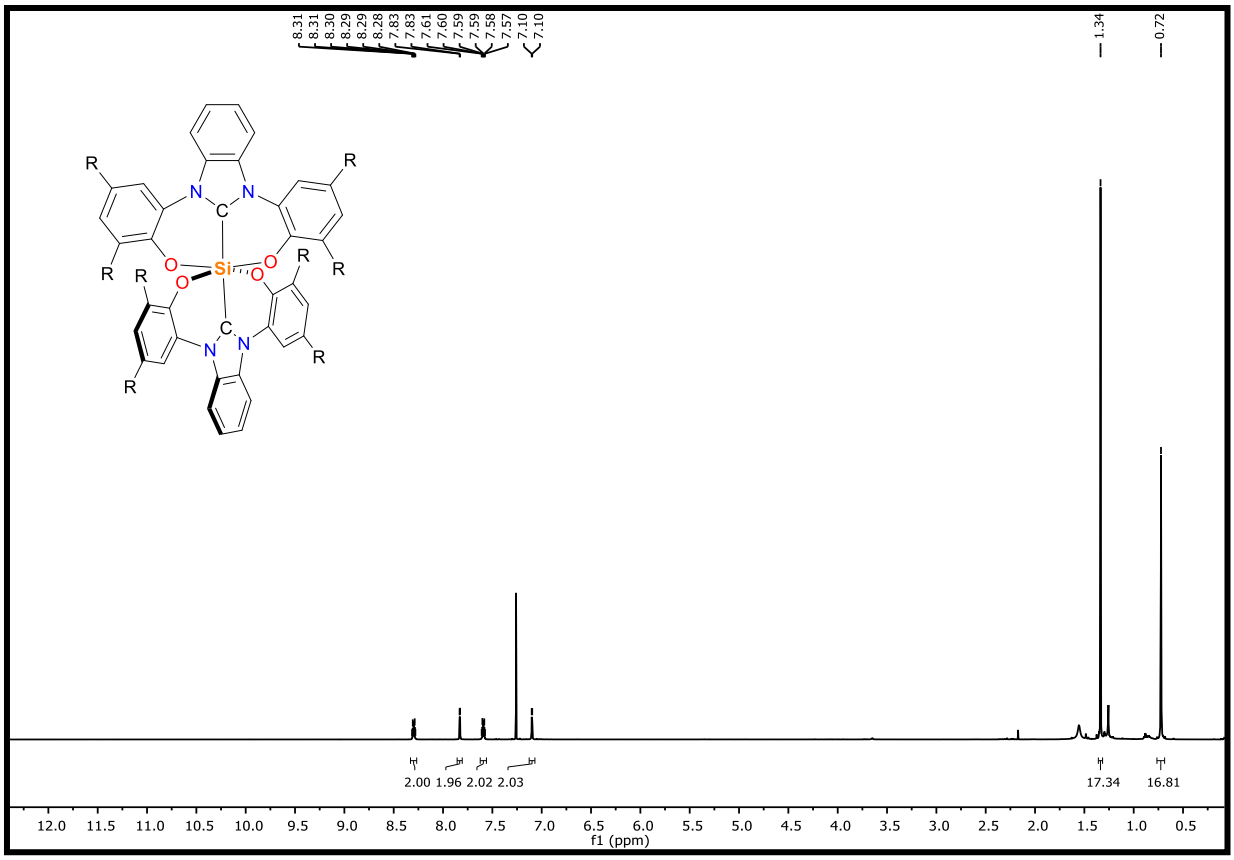

Figure S1. ^{1}H NMR of **Si(OCO)$_2$** in $CDCl_3$.

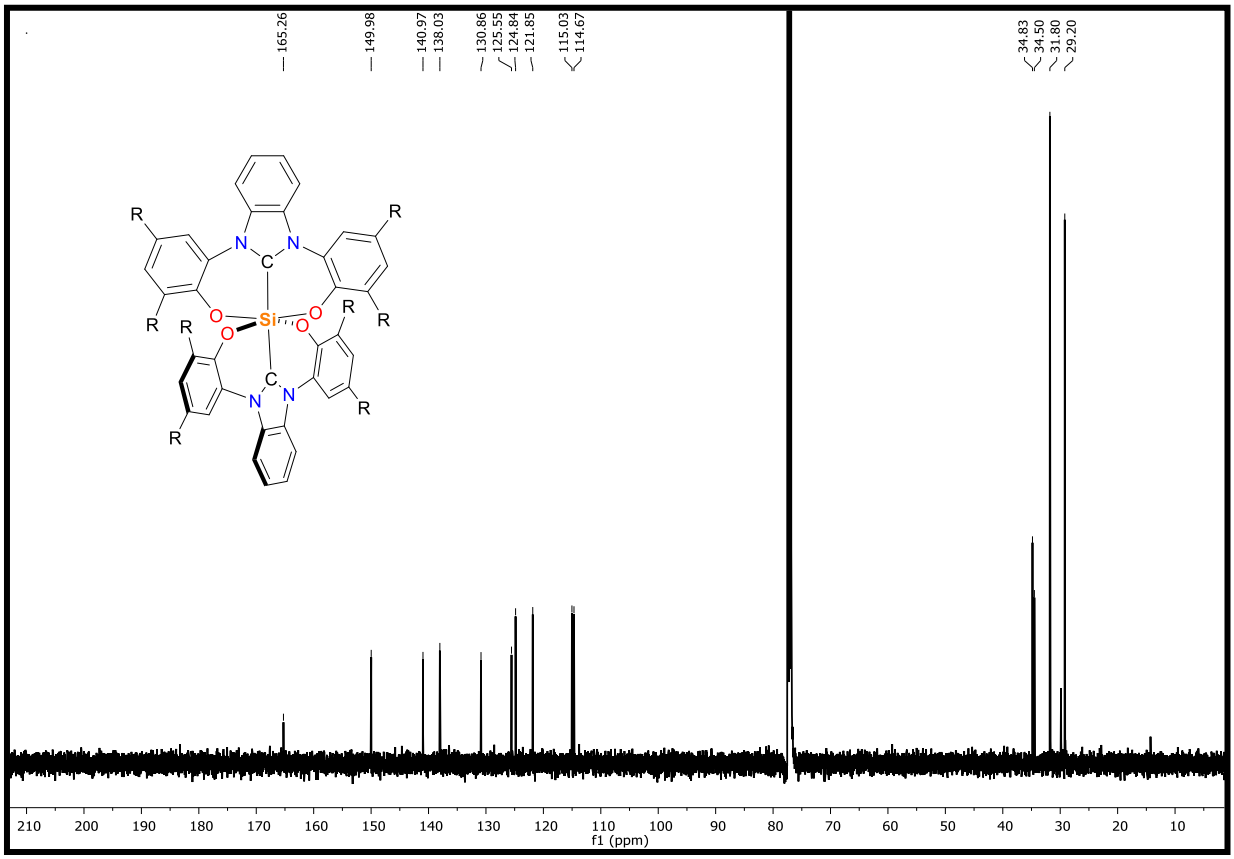

Figure S2. ^{13}C NMR of **Si(OCO)$_2$** in $CDCl_3$.

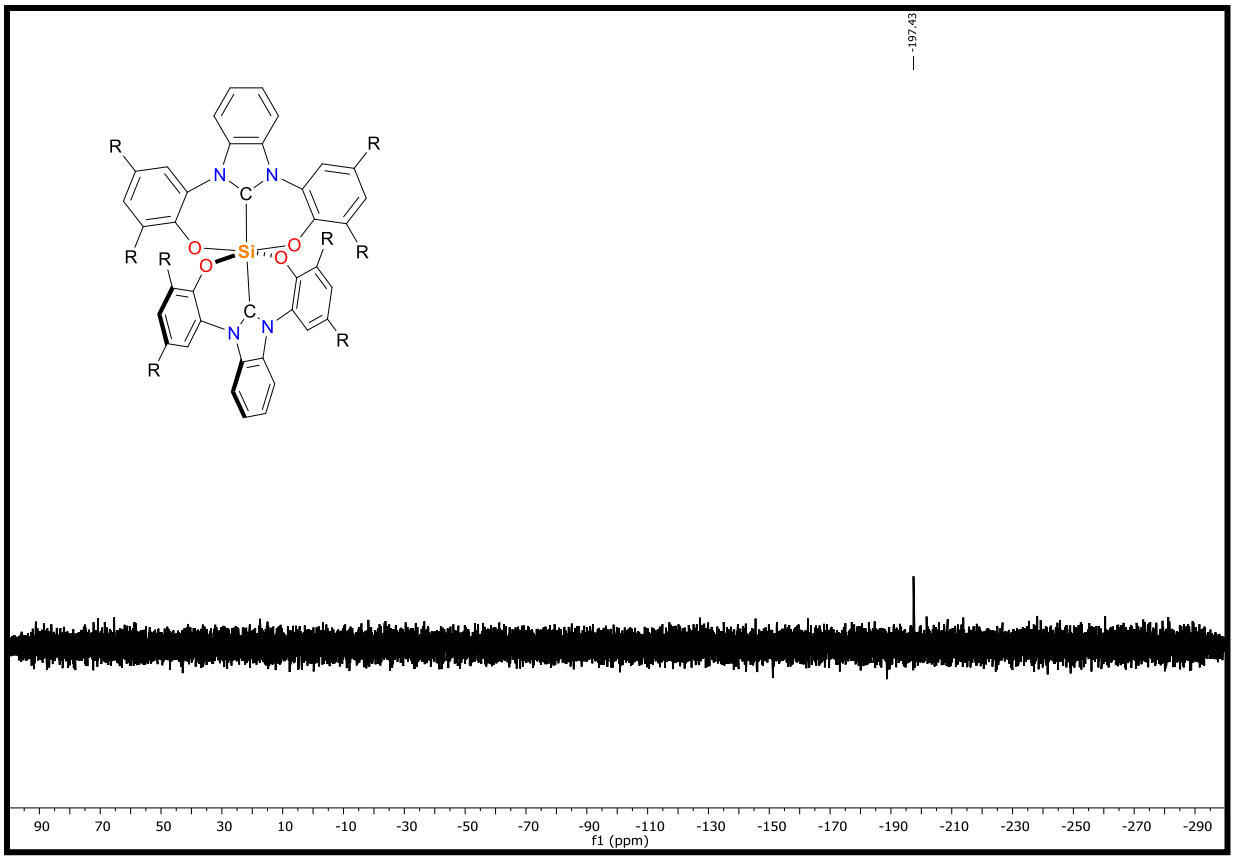

Figure S3. ^{29}Si NMR of **Si(OCO)$_2$** in $CDCl_3$.

X-ray crystallography

The crystals were placed in oil, and a single crystal was selected, mounted on a glass fiber and placed in a low-temperature N_2 stream. X-ray diffraction data collection was carried out on a Bruker PHOTON III DUO CPAD diffractometer equipped with an Oxford Cryosystem liquid N_2 device, using Mo-Kα radiation (λ = 0.71073 Å). The crystal-detector distance was 38mm. The cell parameters were determined (APEX3 software)[2] from reflections taken from 1 set of 180 frames at 1 second exposure. The structure was solved using the program SHELXT-2018.[3] The refinement and all further calculations were carried out using SHELXL-2018.[4] The H-atoms were included in calculated positions and treated as riding atoms using SHELXL default parameters. The non-H atoms were refined anisotropically, using weighted full-matrix least-squares on F^2. A semi-empirical absorption correction was applied using SADABS in APEX3;[2] transmission factors: T_{min}/T_{max} = 0.7231/0.7456.

For the compound, the SQUEEZE instruction in PLATON was applied.[5] The residual electron density was assigned to 2.5 molecules of the dichloromethane solvent. The methyls C68 C69 C70 C68A C69A C70A of the tertbutyl are disordered over two positions with an occupancy ratio of 0.57/0.43.

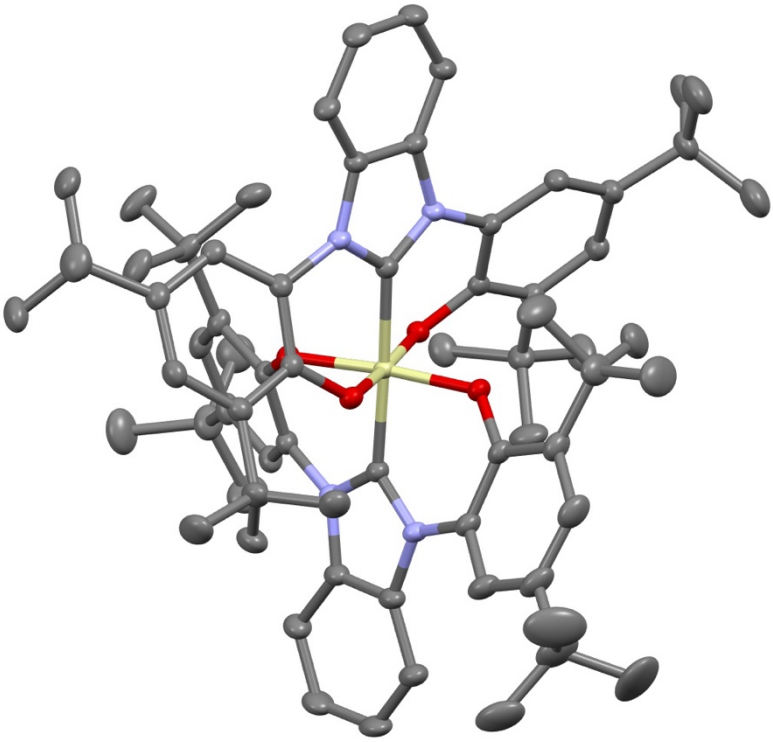

Figure S4. Crystal structure of **Si(OCO)$_2$**. Crystals obtained by DCM/pentane solvent diffusion. Space Group: P-1, Cell: *a* = 13.214 Å, *b* = 14.144Å, *c* = 21.957Å; α = 97.1410(10)°, β = 98.7510(10)°, γ = 113.2650(10)°. CCDC deposition number **2284375**.

Table S1 - Crystal data and structure refinement for **Si(OCO)2**. CCDC deposition number **2284375**

Empirical formula	$C_{72.50}\ H_{93}\ Cl_5\ N_4\ O_4\ Si$	
	'C70 H88 N4 O4 Si,2.5 C H2 Cl2'	
Formula weight	1317.93	
Temperature	120(2) K	
Wavelength	0.71073 Å	
Crystal system, space group	Triclinic, P -1	
Unit cell dimensions	*a* = 13.2142(4) Å	α = 97.1410(10)°
	b = 14.1437(4) Å	β = 98.7510(10)°
	c = 21.9569(7) Å	γ = 113.2650(10)°
Volume	3648.47(19) A^3	
Z, Calculated density	2, 1.200 Mg/m^3	
Absorption coefficient	0.208 mm^{-1}	
F(000)	1402	
Crystal size	0.240 x 0.200 x 0.160 mm	
Theta range for data collection	2.234 to 27.941°	
Limiting indices	-17<=h<=17, -18<=k<=18, -28<=l<=28	
Reflections collected / unique	139273 / 17472 [R(int) = 0.0308]	
Completeness to theta = 25.242	99.9 %	
Absorption correction	Semi-empirical from equivalents	
Max. and min. transmission	0.7456 and 0.7231	
Refinement method	Full-matrix least-squares on F^2	
Data / restraints / parameters	174722 / 18 / 743	
Goodness-of-fit on F^2	1.023	
Final R indices [I>2sigma(I)]	R1 = 0.0486, wR2 = 0.1345	
R indices (all data)	R1 = 0.0561, wR2 = 0.1425	
Extinction coefficient	n/a	
Largest diff. peak and hole	0.784 and -0.790 *e* A^{-3}	

Thermal analysis

Thermogravimetric analyses were carried out on a Q50 systems from TA Instruments under air with a thermal scanning rate of 5°C min^{-1}.

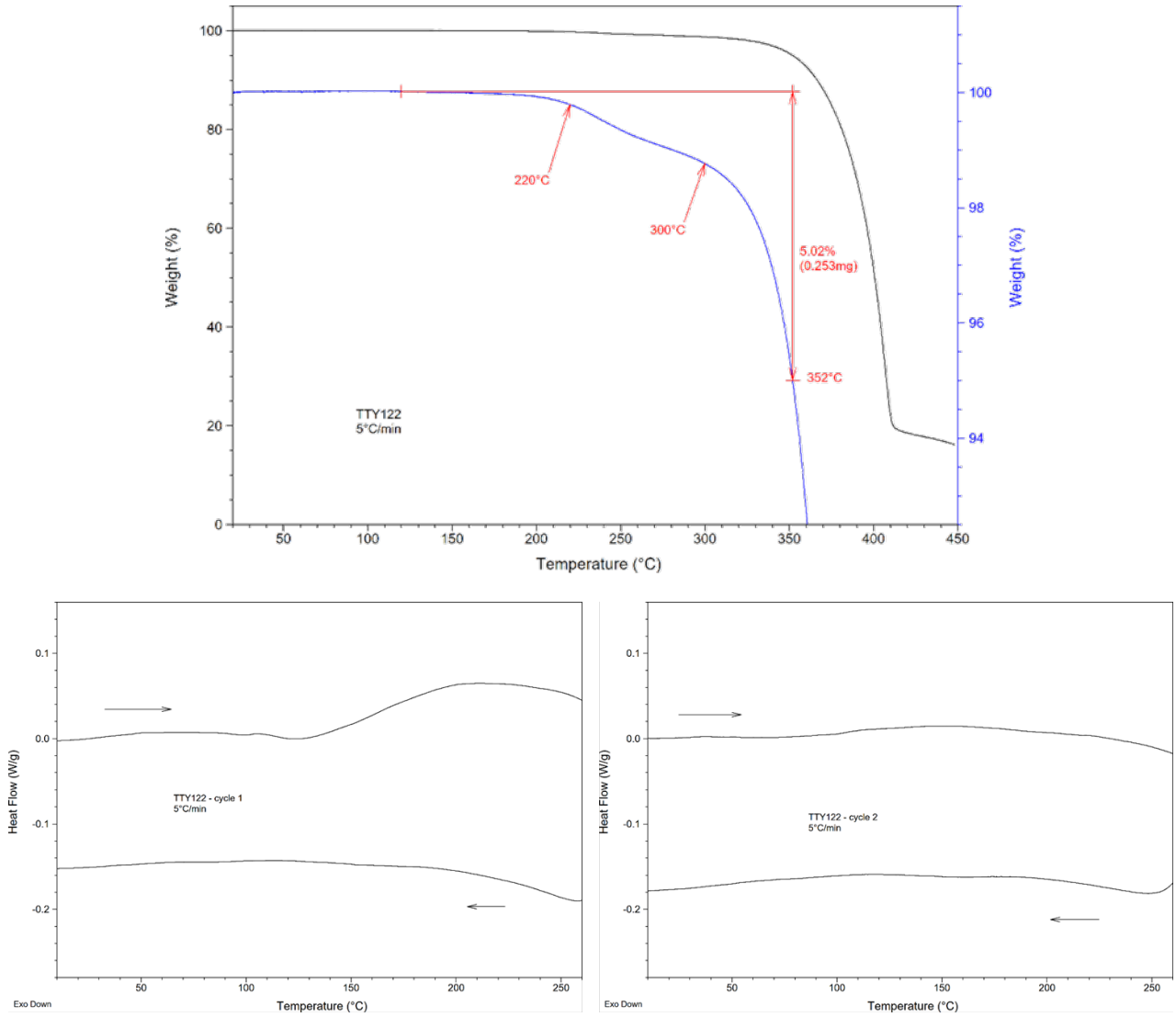

Figure S5. Crystal structure TGA/DSC analysis for **Si(OCO)$_2$**. TGA Q50 from TA instruments (5°C/min, air) (top). POM: Crystalline solid up to 300°C. Weight loss from degradation becomes significant above ca. 220°C. Rapid decomposition occurs above ca. 300°C. 5% weight loss temperature $T_{5\%}$ = 350°C. DSC Q50 from TA instruments (5°C/min endotherm up), cycle 1 (bottom left) and cycle 2 (bottom right). No phase transition observed within the rage of thermal stability.

Electrochemistry

Anhydrous dichloromethane (DCM, Sigma-Aldrich, 99.9%) and tetra-*n*-butylammonium perchlorate (TBAP, Sigma-Aldrich, 99%) were used as received. The working electrode was a glassy-carbon disk electrode (2 mm diameter, Princeton Applied Research GO224). The electrode was polished as already described elsewhere.[6] Before experiments, the electrode was further polished with a 0.05 µm polycrystalline diamond suspension (Buehler, MetaDI) and electrochemically activated in the background solution by means of several voltammetric cycles at 0.5 V s^{-1} between the anodic and the cathodic solvent/electrolyte discharges,

until the expected quality features were attained.[7] A platinum wire served as the counter electrode and a silver wire, separated from the main electrolytic compartment by a Vycor® frit, was used as a quasi-reference electrode. At the end of each experiment, its potential was calibrated against the ferricenium/ferrocene couple (Fc), used as an internal redox standard. Therefore, all the potentials against Fc. The cyclic voltammetry (CV) experiments were carried out in DCM/0.1 M TBAP under an Ar atmosphere, using a 1 mM concentration for the electroactive compound. An SP300 Electrochemical Workstation (BioLogic) was used. For the CV experiments, we employed the feedback correction to minimize the ohmic drop between the working and the reference electrodes.

In the negative-going scan **Si(OCO)$_2$** shows an irreversible reduction process R_1 at -2.30 V vs Fc, which is assigned to the reduction of the ligand. Whereas, in the positive-going scan, it shows three oxidation processes O_n (where n denotes the oxidation process 1-3) at -0.50, 0.23, and 0.64 V vs Fc, respectively. It is worth mentioning that the latter processes appear only when the potential is first scanned in the negative-going direction and then reverted. Therefore, these processes can be also assigned to the oxidation of the ligand and not of the Si core.

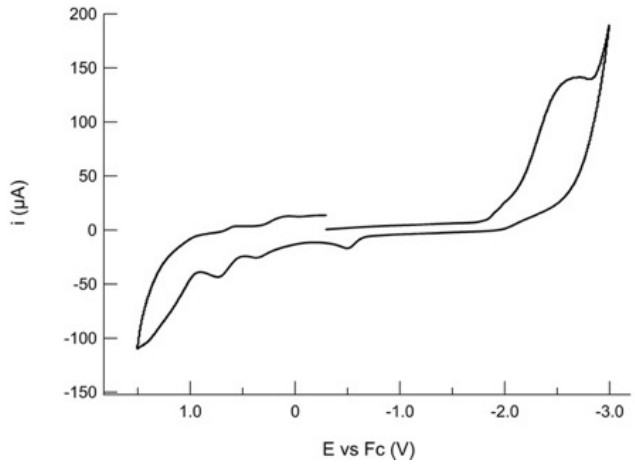

Figure S6. CV of **Si(OCO)$_2$** carried out in CH_2Cl_2/0.1 M TBAP. Scan rate 0.2 V s^{-1}.

Table S2. Main electrochemical data of complex **Si(OCO)$_2$**. CVs were carried out in CH_2Cl_2/0.1 M TBAP. The values are referenced to the redox couple ferrocene/ferricenium (Fc|Fc$^+$) as the internal standard.

Complex	$E_{p,O_1}(V)$ [a]	$E^0_{O_2}(V)$ [b]	$E^0_{O_3}(V)$ [b]	$E_{p,R_1}(V)$ [a]
Si(OCO)$_2$	+0.50	+0.23	+0.64	–2.30

[a] Irreversible processes. Only the peak potential, E_p, is reported. [b] Weakly reversible process for scan rate higher than 0.2 Vs^{-1}. The formal potential, E^0, was calculated as the average of the cathodic and anodic peak of the process.

Photophysical studies

Absorption spectra of fluid solution samples were measured on a Varian Cary 100 double-beam UV–VIS spectrophotometer and baseline corrected. Steady-state emission spectra were recorded on a Horiba Jobin–Yvon IBH FL-322 Fluorolog 3 spectrometer equipped with a 450 W xenon arc lamp, double-grating excitation, and emission monochromators (2.1 nm mm^{-1} of dispersion; 1200 grooves mm^{-1}) and a Hamamatsu R13456 red sensitive Peltier-cooled PMT detector. Emission and excitation spectra were corrected for source intensity (lamp and grating) and emission spectral response (detector and grating) by standard correction curves. Time-resolved measurements were performed using either the time-correlated single-photon counting (TCSPC) or the Multi Channel Scaling (MCS) electronics option of the TimeHarp 260 board installed on a PicoQuant FluoTime 300 fluorimeter (PicoQuant GmbH, Germany), equipped with a PDL 820 laser pulse driver. A pulsed laser diode LDH-P-C-375 (λ = 375 nm, pulse full width at half maximum FWHM <40 ps) driven at repetition rate in the range 50 kHz–40 MHz) was used to excite the samples either with either single pulse or burst mode. Excitation source was mounted directly on the sample chamber at 90°. The photons were collected by a PMA Hybrid-07 single photon counting detector. The data were acquired by using the commercially available software EasyTau II (PicoQuant GmbH, Germany), while data analysis was performed using the built-in software FluoFit (PicoQuant GmbH, Germany). All the PLQYs on samples were recorded at a fixed excitation wavelength by using a Hamamatsu Photonics absolute PLQY measurements system Quantaurus QY equipped with CW Xenon light source (150 W), monochromator, integrating sphere, C7473 photonics multi-channel analyzer and employing the commercially available U6039-05 PLQY measurement software (Hamamatsu Photonics Ltd., Shizuoka, Japan). All measurements were repeated five times at the excitation wavelength λ_{exc} = 320 nm, unless otherwise stated.

For time resolved measurements, data fitting was performed by employing the maximum likelihood estimation (MLE) methods and the quality of the fit was assessed by inspection of the reduced χ^2 function and of the weighted residuals. For multi-exponential decays, the intensity, namely *I(t)*, has been assumed to decay as the sum of individual single exponential decays (eqn. 1):

$$I(t) = \sum_{i=1}^{n} \alpha_i exp\left(-\frac{t}{\tau_i}\right) \quad (Eqn. 1)$$

where τ_i are the decay times and α_i are the amplitude of the component at $t = 0$. In the tables, the percentages to the pre-exponential factors, α_i, are listed upon normalization. Intensity average lifetimes were calculated by using the following equation (eqn. 2):

$$\bar{\tau} = \frac{a_1\tau_1^2 + a_2\tau_2^2}{a_1\tau_1 + a_2\tau_2} \quad (Eqn. 2)$$

All the solvents employed were Merck Uvasol® spectrophotometric grade. Deaerated samples were prepared by the freeze-pump-thaw technique by using a custom quartz cuvette equipped with a Rotaflo® stopcock.

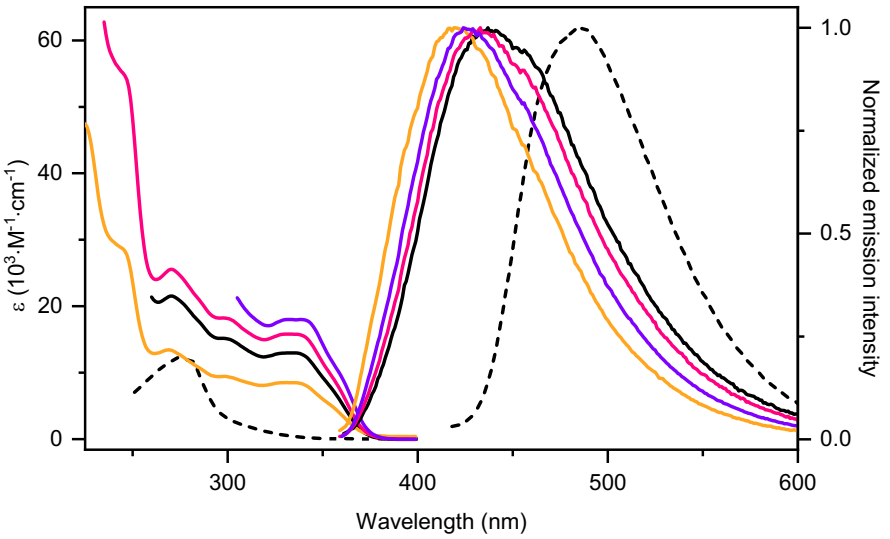

Figure S7. UV-vis absorption and photoluminescence emission in dilute solvents (2×10^{-5} M) for **Si(OCO)$_2$** (solid) and **(OCO)H$_3$** (dashed). CH_2Cl_2 (black), MeOH (yellow), THF (magenta), toluene (violet). Emission spectra were recorded upon excitation at λ_{exc} = 320 nm.

Table S3. Photophysical properties of **Si(OCO)$_2$** and **(OCO)H$_3$** in dilute air-equilibrated organic solvents (2.0×10^{-5} M) at room temperature. Radiative and non-radiative rate constants were determined with the equations $k_r = PLQY/\tau$ and $k_{nr} = (1 - PLQY)/\tau$ respectively. *sh* denotes a shoulder. *br* denotes a broad signal.

compound	solvent	λ_{max} (ε) [nm, (10^3 M^{-1} cm^{-1})]	λ_{em} [nm]	PLQY (%)	τ_{obs} [ns]	$\bar{\tau}_{obs}$ [ns]	k_r [10^8 s^{-1}]	k_{nr} [10^8 s^{-1}]
(OCO)H$_3$	CH_2Cl_2	**274** (12.251), 280 (12.011)	492, 525, 567	6	1.87	-	0.05	5.29
Si(OCO)$_2$	CH_2Cl_2	**271** (21.549), 299*sh* (15.024), 332 (12.878)	**437**, 456*sh*	2	0.21	-	0.96	46.89
	MeOH	245*sh* (29.377) 269*sh* (14.188) 301*sh* (10.085) 336*sh br* (9.225)	**420**	4	2.59 (52%) 0.23 (48%)		-	-
	THF	246*sh* (54.682) 270 (25.525) 299*sh* (18.180) 335*br* (15.760)	**430**	2	0.20	-	0.99	48.28
	Toluene	336*br* (17.923)	**426**	4	0.50	-	0.79	18.86

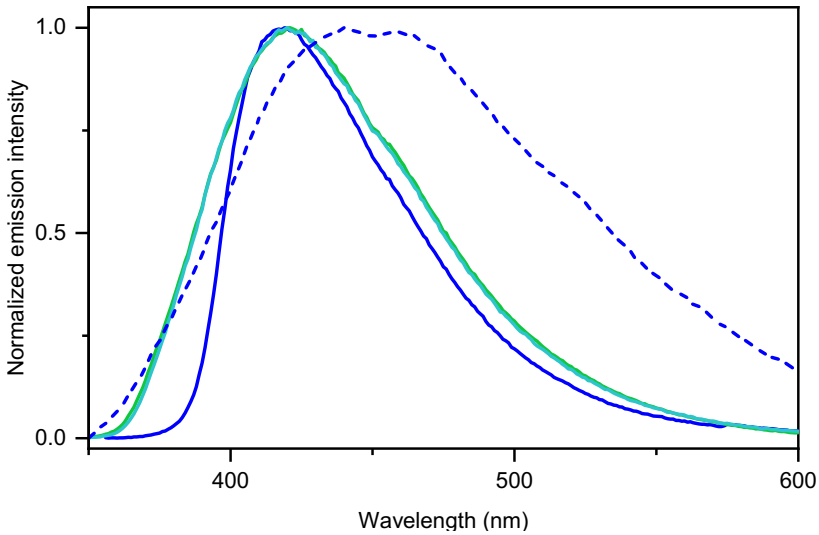

Figure S8. Photoluminescence emission for **Si(OCO)$_2$** (solid) and **(OCO)H$_3$** (dashed) as crystalline powders (blue), thin film in PMMA (green) and PS (aqua). Spectra were recorded upon excitation at λ_{exc} = 320 nm.

Computational details

Ground state and lowest-lying singlet excited state geometries were optimized by means of density functional and time-dependent density functional calculations. The parameter-free hybrid functional PBE0[8] was employed along with the standard valence double-ζ polarized basis set 6-31G(d,p) for C, H, N, O and Si. All the optimizations were done in vacuo while time-dependent calculations were done also in the presence of the solvents employed in the photophysical characterization, described by a polarizable continuum model (PCM)[9]. The nature of all the stationary points was checked by computing vibrational frequencies and all the geometries were found to be true minima. In order to simulate the absorption electronic spectrum down to about 250 nm the lowest 30 singlet excitation energies were computed by means of time-dependent density functional calculations. All the calculations were done with Gaussian 16.[10]

Table S4. Properties of some of the more intense electronic transitions computed for the methyl-substituted analogue **Si(O^{Me}CO^{Me})$_2$**.

S_n		E [eV]	λ [nm]	f		
S_1 S_2	E	3.559	348	0.0746	194→196,197 195→196,197	43% 55%
S_8	A	4.011	309	0.0886	192,193→196,197	98%
S_9 S_{10}	E	4.387	283	0.0551	194→200,201 195→200,201	36% 47%
S_{12}	B	4.424	280	0.2049	194→199 195→198	35% 56%
S_{13} S_{14}	E	4.517	274	0.0926	190→196,197 191→196,197	34% 56%

Table S5. Selected geometric parameters [Å,°] for the ground state S_0 and the first singlet excited state S_1 of the methyl-substituted analogue **Si(O^{Me}CO^{Me})$_2$**. Labels can be found in the enclosed scheme.

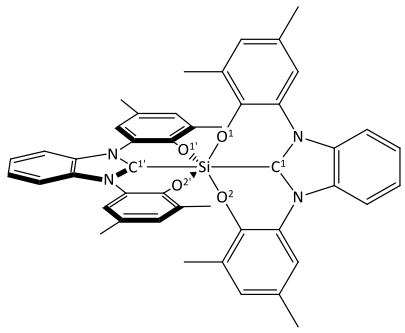

	S_0	S_1
Si–O^1	1.790	1.950
Si–O^2	1.790	1.741
Si–C^1	1.920	1.868
Si–O$^{1'}$	1.790	1.792
Si–O$^{2'}$	1.790	1.805
Si–C$^{1'}$	1.920	1.937

	S_0	S_1
O^1–Si–O^2	176.23	177.33
O^1–Si–C^1	88.12	88.48
O^1–Si–O$^{1'}$	90.06	88.06
O^1–Si–O$^{2'}$	90.06	83.50
O^1–Si–C$^{1'}$	91.88	86.83
O^2–Si–C^1	88.12	92.21
O^2–Si–O$^{1'}$	90.06	94.48
O^2–Si–O$^{2'}$	90.06	93.88
O^2–Si–C$^{1'}$	91.88	92.48
C^1–Si–O$^{1'}$	91.88	92.72
C^1–Si–O$^{2'}$	91.88	93.75
C^1–Si–C$^{1'}$	180	175.31
O$^{1'}$–Si–O$^{2'}$	176.23	169.22
O$^{1'}$–Si–C$^{1'}$	88.12	86.94
O$^{2'}$–Si–C$^{1'}$	88.12	85.91

As expected, the optimized S_1 geometry shows a drastic loss of symmetry, since the HOMO–LUMO transition leads to an asymmetric occupation of degenerate orbitals. In the C_1 optimized structure one of the two ligand is asymmetrically coordinated to the silicon atom: one of the Si–O bond length is elongated with respect to the ground state structure (+0.160 Å), with a corresponding shortening of the C–O bond length to a value typical of double bonds (1.276 Å). At the same time, in the same ligand a shortening of the other Si–O bond (–0.049 Å) and of the Si–C bond (–0.052 Å) is observed. On the other hand, the geometry of the other ligand is almost unchanged from the ground state. The silicon atom retains its octahedral coordination, displaying a long Si···O interaction and a distortion of the bond angles (with large deviations from the ideal values of 90 and 180°, see Table S4).

Table S6. Properties of the lowest energy absorption transition $S_0 \rightarrow S_1$ and the vertical emission $S_1 \rightarrow S_0$ computed in the presence of different solvents.

solvent	absorption			emission	
	E [eV]	λ [nm]	*f*	*E* [eV]	λ [nm]
MeOH	3.702	335	0.1295	2.813	441
CH_2Cl_2	3.676	337	0.1320	2.778	446
THF	3.671	338	0.1292	2.769	448
toluene	3.614	343	0.1233	2.684	462

Some of the calculations have been performed in the presence of the solvents employed in the photophysical characterization (toluene, tetrahydrofuran, dichloromethane and methanol, in order of increasing polarity, see Table S5). Due to the small change in the dipole moment computed for the $S_0 \rightarrow S_1$ transition and to the nonpolar nature of the ground state of S_4 symmetry, this absorption shows only a limited shift to higher energies on increasing solvent polarity (from 343 nm in toluene to 335 nm in methanol, a shift of ca. 700 cm^{-1}). The effect on the emission wavelength appears to be more pronounced (from 462 to 441 nm, a shift of 1040 cm^{-1}), as a consequence of the higher difference in the dipole moment of the states involved in the transition.

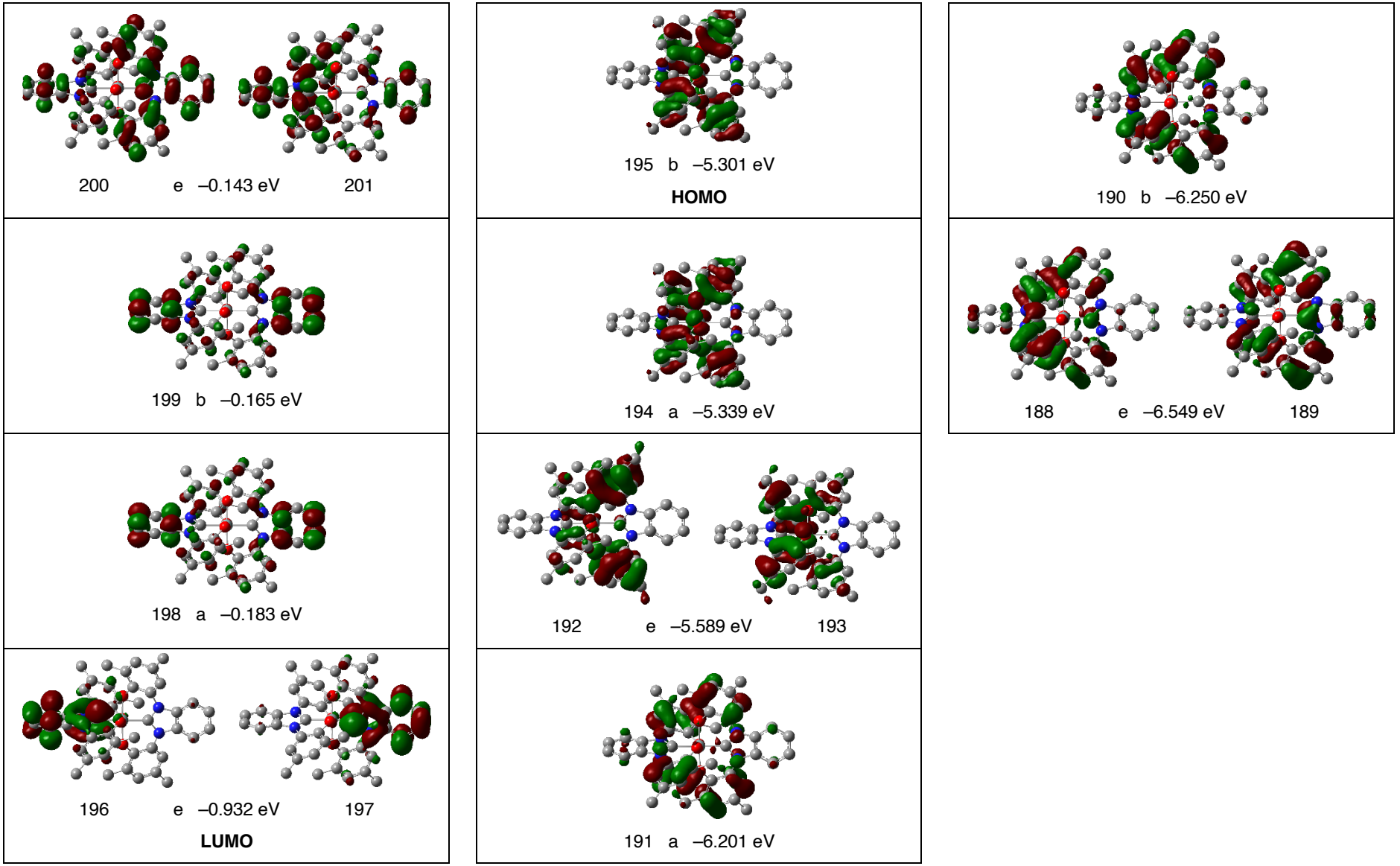

Figure S9. Relevant molecular orbitals computed for the methyl-substituted analogue **Si(O^{Me}CO^{Me})$_2$**. Hydrogen atoms are omitted for clarity.

Fabrication and characterization of OLEDs

Organic materials purchased from Shine Materials Technology were subjected to temperature-gradient sublimation in a high vacuum before use. After a cleaning procedure of ultrasonication of the ITO-coated glass in deionized water and organic solvents, the ITO substrate was pretreated with plasma for 5 minutes. The organic and metal layers were deposited by thermal evaporation in a vacuum chamber with a base pressure of < 10^{-6} Torr. Device fabrication was completed in a single cycle without breaking the vacuum. The deposition rate of organic materials was kept at around 0.1 nm s^{-1}. The active area was defined by the shadow mask (2 × 2 mm^2). Current density-voltage-luminance characterization was done using two Keysight B2901A current source-measure units equipped with a calibrated Si-photodiode. The electroluminescent spectra of the devices were recorded using an Ocean Optics spectrometer (Ocean Optics 2000).

Structure and performance of OLEDs

Device architecture incorporates a composite structure of hole injection layer (HIL) composed of a 1,1-bis[(di-4-tolylamino)phenyl]cyclohexane (TAPC) layer, and a TAPC doped with MoO_3 layer, enabling a smooth hole injection from the ITO anode to the organic layer. Furthermore, 4,4',4"-tris(carbazol-9-yl)-triphenylamine (TCTA) was used as the hole transport layer, aiming to promote smooth hole injection from the hole transporting layer (HTL) into the emitting layer (EML). Considering the carrier transport and energy transfer, we selected bipolar N,N'-dicarbazolyl-3,5-benzene (mCP) as the host material for the synthesized blue emitters in the EML. Conversely, as the electron transporting layer (ETL) situated between the EML and the lithium fluoride (LiF)-electron injection layer (EIL), we selected a wide triplet-energy-bandgap material, 1,3,5-tri[(3-pyridyl)-phen-3- yl]benzene (TmPyPB). As a result, the optimized architecture for the tested devices was set to ITO (120 nm)/TAPC:MoO_3 20 wt.% (5 nm)/TAPC (25 nm)/TCTA (10 nm)/ mCP:Si(OCO)2 (20 nm)/TmPyPB (50 nm)/LiF (0.8 nm)/Al (120 nm), where the aluminum was used as the cathode. The corresponding chemical structures of the used materials, the schematic structures, and the energy level diagram of the fabricated OLEDs are presented in Fig. S10.

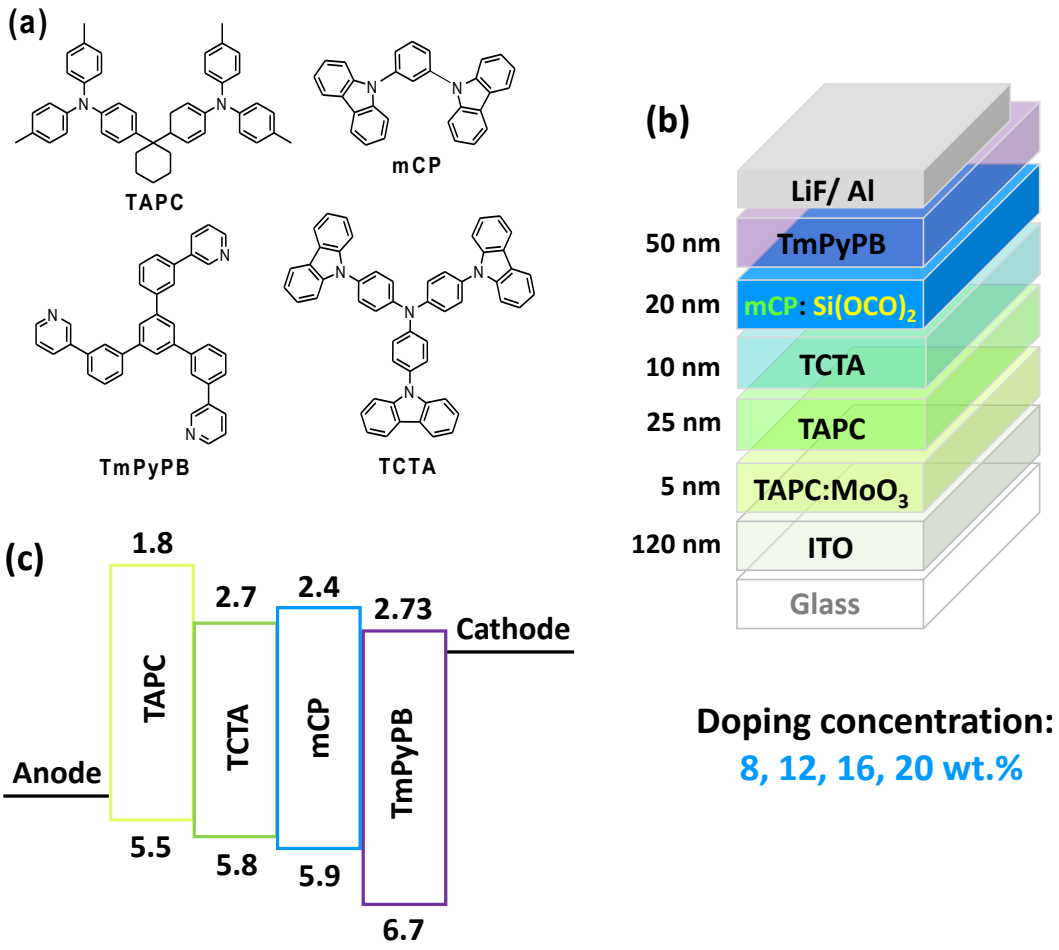

Figure S10. (a) Structural drawings of the materials used in OLEDs, (b) schematic structures of the fabricated OLEDs, (c) energy level diagram of the device.

Table S7. EL characteristics of the devices with different doping concentrations.

Device		**A**	**B**	**C**	**D**
Doping concentration (wt.%)		**8**	**12**	**16**	**20**
External quantum efficiency (%)	[a]	1.2	1.3	1.3	1.3
	[b]	1.1	1.3	1.3	1.3
Luminance efficiency (cd/A)	[a]	0.7	0.8	0.8	0.8
	[b]	0.7	0.7	0.8	0.8
Power efficiency (lm/W)	[a]	0.5	0.6	0.6	0.5
	[b]	0.4	0.5	0.5	0.5
V_{on} (V)	[c]	3.6	3.7	3.8	3.8
FWHM (nm)	[b]	81	81	81	82.5
Max. Luminance (cd/m^2)		2666 [10.6]	2566 [10.6]	2290 [10.8]	2515 [10.6]
CIE1931 Coordinates (x, y)	[b]	(0.18, 0.13)	(0.18, 0.12)	(0.18, 0.12)	(0.18, 0.12)

[a] Maximum efficiency; [b] measured at 10^2 cd/m^2; [c] turn-on voltage measured at 1 cd/m^2.

References

[1] S. Bellemin-Laponnaz, S. Dagorne, R. Dümpelmann and P. Steffanut, *Chimia*, 2014, **68**, 500.

[2] "M86-EXX229V1 APEX3 User Manual", Bruker AXS Inc., Madison, USA, 2016.

[3] G. M. Sheldrick, *Acta Cryst.* 2015*,* **A71**, 3-8.

[4] G. M. Sheldrick, *Acta Cryst.* 2015, **C71**, 3-8.

[5] A. L. Spek, *J. Appl. Cryst.* 2003, **36**, 7-13.

[6] S. Antonello, M. Musumeci, D. D. M. Wayner and F. Maran, *J. Am. Chem. Soc.*, 1997, **119**, 9541–9549.

[7] A. Belèn-Meneses, S. Antonello, M. C. Arévalo and F. Maran, *Electroanalysis*, 2006, **18**, 363–370.

[8] Called PBE1PBE in Gaussian. C. Adamo and V. Barone, *J. Chem. Phys.*, 1999, **110**, 6158–6170.

[9] G. Scalmani and M. J. Frisch, *J. Chem. Phys.*, 2010, **132**, 114110.

[10] Gaussian 16 (revision A.03), Gaussian Inc., Wallingford, CT, 2016, https://gaussian.com/.